# Magnetic coupling constants and vibrational frequencies by extended broken symmetry approach with hybrid functionals

D. Bovi and L. Guidoni

Citation: J. Chem. Phys. **137**, 114107 (2012); doi: 10.1063/1.4752398
View online: http://dx.doi.org/10.1063/1.4752398
View Table of Contents: http://jcp.aip.org/resource/1/JCPSA6/v137/i11
Published by the American Institute of Physics.

# Magnetic coupling constants and vibrational frequencies by extended broken symmetry approach with hybrid functionals

D. Bovi[1] and L. Guidoni[2,a)]
[1]*Physics Department, La Sapienza - University of Rome, Rome, Italy*
[2]*Department of Physical and Chemical Sciences, University of L'Aquila, L'Aquila, Italy*

(Received 7 June 2012; accepted 29 August 2012; published online 20 September 2012)

The description of the electronic structure and magnetic properties of multi-centers transition metal complexes, especially of mixed-valence compounds, still represents a challenge for density functional theory (DFT) methods. The energies and the geometries of the correctly symmetrized low-spin ground state are estimated using the Heisenberg-Dirac-van Vleck spin Hamiltonian within the extended broken symmetry method introduced by Marx and co-workers [Nair *et al.*, J. Chem. Theory Comput. **4**, 1174–1188 (2008)]. In the present work we extend the application of this technique, originally implemented using the DFT+U scheme, to the use of hybrid functionals, investigating the ground-state properties of di-iron and di-manganese compounds. The calculated magnetic coupling and vibrational properties of ferredoxin molecular models are in good agreements with experimental results and DFT+U calculations. Six different mixed-valence Mn(III)–Mn(IV) compounds have been extensively studied optimizing the geometry in low-spin, high-spin, and broken-symmetry states and with different functionals. The magnetic coupling constants calculated by the extended broken symmetry approach using B3LYP functional presents a remarkable agreement with the experimental results, revealing that the proposed methodology provides a consistent and accurate DFT approach to the electronic structure of multi-centers transition metal complexes. © *2012 American Institute of Physics*. [http://dx.doi.org/10.1063/1.4752398]

## I. INTRODUCTION

Multi-center transition metal (TM) complexes have an important role in different fields of biology and materials science. They are present as catalytic and redox centers in many metalloenzymes and electron-transport proteins such as ferredoxin (Fd),[1–3] hydrogenases,[4–7] copper-based enzymes,[8] and photosynthetic complexes.[9–11] They also play an important role in the research of biomimetic inorganic molecular catalysts for water oxidation[12,13] and hydrogen production.[14,15] Theoretical calculations are a valuable tool to evaluate geometrical and spectroscopic parameters of such complexes with the aim to aid rationalization and interpretation of the experimental observations. As demonstrated by several examples present in the literature (see Refs. 16 and 17 and references therein) electronic structure calculations may elucidate different issues of multi-center transition metal complexes, such as the role of the ligands on the metal redox states, the catalytic strategies, and the electron transfer properties, providing the grounds for the interpretation of structural, thermodynamic, kinetic, and spectroscopic data. Post-Hartree Fock correlated methods are still a challenge for multi-center TM complexes and the most used technique for medium and large size system remains density functional theory (DFT).[18,19] Recent calculations on gas phase models of the oxygen evolving complex[20] were able to suggest the location of protons and the magnetic interaction pattern on the catalytic Mn cluster for water oxidation of Photosystem II.[21] In the case of inorganic systems, a recent combination between x-ray absorption data and *ab initio* molecular dynamics techniques revealed the protonation state in solution of $\mu$-oxo bridges in molecular models for artificial photosynthesis.[22]

Despite the wide application range, density functional theory calculations still suffer from two main limitations in describing the electronic structure of multi-center TM complexes. The first major problem is the choice of the approximate exchange-correlation functional. Using the generalised gradient approximation (GGA) the dominating term in the energy functional is the Coulomb repulsion that makes the orbitals localization more difficult.[23,24] In addition these functionals may suffer also from static correlation errors that discourage the formation of open-shell electron states usually possible by the high degeneracy of the *d*-orbitals. On the other hand the HF approach suffers from the opposite drawback, preferring parallel spin configurations and therefore leading to an excessive disposition for localized high-spin (HS) state.[25] In both cases the results might provide an erroneous description of the magnetic properties of the complexes.[26] The second problem affecting Kohn-Sham (KS)-DFT calculations on multi-center TM complexes is represented by the fact that the Kohn-Sham scheme is intrinsically a one-determinant theory which is not suitable to properly describe open-shell spin multiplets, which are often found as ground state of these complexes.[26]

a)Also at Via Campo di Pile, 64100 L'Aquila, Italy. Electrnoic mail: leonardo.guidoni@univaq.it. URL: http://bio.phys.uniroma1.it.

 

Many efforts have been made so far to improve the performances of exchange-correlation functionals on TM complexes. In particular, the use of hybrid functionals, based on a partial contribution of exact Fock exchange, represents a good choice to promote the localization of singly occupied valence molecular orbitals.[27–29] An alternative and effective approach has been proposed by introducing an on-site repulsion term (Hubbard-U term) in the Hamiltonian.[30–33] The latter approach provides an electron localization effect similar to that observed with hybrid functionals, with the advantage of being more easily and efficiently implemented in plane wave schemes and in *ab initio* molecular dynamics.[22,34]

In multi-center TM complexes where each metal center has near half filled *d*-orbitals, thanks to Hund's rule, the parallel alignment of the valence electrons' spins is usually preferred on-site and leads to a resulting local high-spin configuration on each metal center. These local spinors may interact to each other either in ferromagnetic or in antiferromagnetic (or ferrimagnetic) way, leading to total HS or low-spin (LS) ground states, respectively. The LS state is often globally an open-shell spin singlet (S=0) state, although formed by unpaired high-spin states on-sites. The correct representation of such spin state is beyond the one-determinant picture of DFT because of the missing appropriate symmetrization of the spinor part. A widely used technique to circumvent this problem is to evaluate different single determinant magnetic configurations using the so-called broken-symmetry (BS) approach.[35–37] The broken-symmetry states suffers anyway from spin contamination, since they are not exact eigenstates of the total spin $S^2$ operator;[17] anyway, they often represent in many cases a good approximation of the ground-state electron density. An alternative approach to access the LS ground state with the correct spin symmetry is represented by the so-called extended broken-symmetry (EBS) method proposed by Marx and co-workers[38] and successfully used in combination with the DFT+U approach for calculating geometrical, energetic, and magnetic properties of di-nuclear iron complexes.[39,40] The approach is based on the reconstruction of LS energy surface trough an Heisenberg-like Hamiltonian depending on the empirical coupling parameter *J*. The parameter can be estimated by performing two independent single determinant HS and BS calculations.[34,38] So far the application of EBS was limited to a couple of iron-sulfur complexes and to the use of DFT+U scheme in plane waves.[34,38–41]

In the present work we investigate the capability of EBS in combination with hybrid functionals to describe the geometry and energetics of di-nuclear iron and manganese complexes. Our results will be also compared with those obtained using other theoretical approaches and with the available experimental data. In Sec. II we review the EBS formalism and we apply it to the calculation of harmonic vibrational frequencies. In Sec. III we present the obtained results and report the features and the accuracy of the EBS approach in combination with hybrid functionals, focusing on the geometrical and magnetic properties of two classes of systems: ferredoxin complex models that were previously investigated by EBS DFT+U calculations, and mixed-valence di-manganese complexes for which an extensive BS study has been done.[42]

## II. METHODS

Due to the inadequacy of Kohn-Sham formulation of DFT to describe multi determinant ground states, the open-shell LS ground state of several TM cluster requires in principle the use of multideterminantal methods. Despite this drawback, the so-called BS[35,36] implementation of DFT can provide reasonably good molecular geometries and energies even if the correct spin symmetry is not satisfied by the one-determinant wave function. A simple, alternative proposal to go beyond this approach is the EBS method,[38–40] where the description of the LS ground-state properties is achieved through the evaluation of the exchange coupling constant *J* using separated calculations performed on BS and on HS states. In the present section we will review the computational methods to evaluate the exchange coupling constant and its use in the EBS method scheme. The EBS approximation is therefore extended to the LS Hessian matrix to evaluate harmonic vibrational frequencies in LS state. Computational details of the Fe- and Mn-based complexes are also reported.

### A. Evaluation of exchange coupling constant *J*

The magnetic coupling between the two on-site high-spin states in TM dimers can be described at phenomenological level by the Heisenberg-Dirac-van Vleck spin Hamiltonian[43–45]

$$\hat{H} = -2J\hat{S}_A\hat{S}_B, \tag{1}$$

where $\hat{S}_A$ and $\hat{S}_B$ are the spin operators of the resulting magnetic momentum on the metal center *A* and *B*, while *J* is the exchange coupling constant between the two magnetic centers. The phenomenological description of Eq. (1) is valid in the strong exchange coupling limit[46] $|J| \gg 1$ for homovalent or heterovalent magnetic dimers as demonstrated for the case of Mn dimers.[47,48] The Hamiltonian could be also generalised to polynuclear magnetic centers.[38] For the binuclear case, defining the total spin operator $\hat{S} = \hat{S}_A + \hat{S}_B$, the Hamiltonian (1) can be reformulated as

$$\hat{H} = -J\left(\hat{S}^2 - \hat{S}_A^2 - \hat{S}_B^2\right) \tag{2}$$

and the energy of a state of total spin *S* is given by

$$E^S = -J[\langle\hat{S}^2\rangle^S - S_A(S_A+1) - S_B(S_B+1)]. \tag{3}$$

In case of pure spin states, the $\hat{S}^2$ operator in Eq. (3) can be replaced by its corresponding eigenvalue. In DFT the one-determinant representations of the antiferromagnetic configurations, the BS states, are not eigenstates of $\hat{S}^2$ since they are "contaminated" by components on higher spin states. Nevertheless, in these cases $\langle\hat{S}^2\rangle$ can be estimated numerically in an approximated way.[39,49,50] The Hamiltonian (1), adopted to describe the magnetic coupling between metal centers, generates an Heisenberg's spin-ladder of eigenstates with *S* ranging from $S_{\min} = |S_A - S_B|$ up to $S_{\max} = S_A + S_B$, where $S_{\max}$ and $S_{\min}$ are the maximum and minimum total spin quantum numbers corresponding to the exact HS and LS eigenstates of Eq. (1), respectively. On the contrary, the BS state does not belong to the Heisenberg's ladder, and due to the higher spin contamination in the antiferromagnetic case its energy

is higher than the LS energy. Due to its symmetry, the HS state is always represented by a single Slater determinant and can be therefore correctly evaluated by DFT. These two latter states can be used together to estimate the coupling constant $J$, using the Yamaguchi formula, obtained combining Eq. (3) for the HS and BS states (see Refs. 51 and 52 and references therein)

$$J = \frac{E^{\mathrm{BS}} - E^{\mathrm{HS}}}{\langle \hat{S}^2 \rangle^{\mathrm{HS}} - \langle \hat{S}^2 \rangle^{\mathrm{BS}}}, \tag{4}$$

where $E^{\mathrm{HS}}$ and $E^{\mathrm{BS}}$ are the total energies of the HS and BS states, respectively.

### B. Extended broken symmetry to access the low-spin energy, forces and Hessian

Beyond the evaluation of the exchange interaction $J$, the knowledge of the HS and BS states can be used to obtain information on all the spin-ladder eigenstates (Eq. (3)) and, in particular, on the LS state.[38–40]

In general the $\langle \hat{S}^2 \rangle$ value, appearing in Eq. (5), can be evaluated using the Löwdin's formulation[49]

$$\langle \hat{S}^2 \rangle = \left( \frac{n^{\alpha}_{\mathrm{mag}} - n^{\beta}_{\mathrm{mag}}}{2} \right) \left( \frac{n^{\alpha}_{\mathrm{mag}} - n^{\beta}_{\mathrm{mag}}}{2} + 1 \right) + n^{\beta}_{\mathrm{mag}} + \Theta, \tag{5}$$

where

$$\Theta = n^{\beta}_{\mathrm{nmag}} + 2 \int \Gamma(\mathbf{r}_1\alpha, \mathbf{r}_2\beta | \mathbf{r}_1\beta, \mathbf{r}_2\alpha) \mathrm{d}\mathbf{r}_1 \mathrm{d}\mathbf{r}_2. \tag{6}$$

In Eqs. (5) and (6), $n^{\alpha}_{\mathrm{mag}}(n^{\beta}_{\mathrm{mag}})$ and $n^{\alpha}_{\mathrm{nmag}}(n^{\beta}_{\mathrm{nmag}})$ are the numbers of unpaired and paired $\alpha(\beta)$ electrons,[53] respectively; $\Gamma(\mathbf{r}_1\sigma_1, \mathbf{r}_2\sigma_2 | \mathbf{r}_1\sigma_2, \mathbf{r}_2\sigma_1)$ is the two-particles density matrix and $\Theta$ is a correction term that arises from the spin contamination due to nonsymmetric spin states and from the overlap between the magnetic orbitals. In the special case of the HS state, that is a pure spin state eigenfunction of the Hamiltonian (1), $\Theta \approx 0$ and $n^{\beta}_{\mathrm{mag}} = 0$, since formula (5) is reduced to the proper eigenvalue $S(S+1)$. In the other cases, when the total spin $S < S_{\mathrm{max}}$, $\Theta > 0$ and $S^2$ has always positive deviation from the exact value.

The equation for the exchange coupling constant (4) can be rewritten in terms of these new quantities[39]

$$J = \frac{E^{\mathrm{BS}} - E^{\mathrm{HS}}}{S^2_{\mathrm{max}} - S^2_{\mathrm{min}} - \Theta^{\mathrm{BS}} + \Theta^{\mathrm{HS}}}. \tag{7}$$

Using Eq. (3) and the latter definition of $J$ (7), the energy of the LS ground state can be written in terms of the HS and BS total energies as its general spin-projected representation[38] (8),

$$E^{\mathrm{LS}} = (1+c)E^{\mathrm{BS}} - cE^{\mathrm{HS}} = \mathcal{P}E^{\mathrm{BS,HS}}, \tag{8}$$

$$c = \frac{S_{\mathrm{max}} - S_{\mathrm{min}} + \Theta^{\mathrm{BS}}}{S^2_{\mathrm{max}} - S^2_{\mathrm{min}} - \Theta^{\mathrm{BS}} + \Theta^{\mathrm{HS}}}. \tag{9}$$

It is possible to exploit the same weighted sum of energies (8) to calculate the energy gradient and Hessian of the LS state assuming the condition that $c$ (9) is nearly constant[38,39] ($\mathrm{d}c/\mathrm{d}R_I = 0$) . In this approximation, Eq. (8) leads directly to the LS forces (Eq. (10))

$$\mathbf{F}^{\mathrm{LS}}_I = (1+c)\mathbf{F}^{\mathrm{BS}}_I - c\mathbf{F}^{\mathrm{HS}}_I \tag{10}$$

and to the LS Hessian

$$\mathbf{K}^{\mathrm{LS}} = (1+c)\mathbf{K}^{\mathrm{BS}} - c\mathbf{K}^{\mathrm{HS}}. \tag{11}$$

Considering the LS potential energy surface at its equilibrium geometry, in harmonic approximation it is possible to use the LS Hessian under mass weighted transformation ($\tilde{K}_{ij} = K_{ij}/\sqrt{m_i m_j}$) to calculate vibrational frequencies and normal modes of LS state.

### C. Computational details

The DFT calculations for the HS and BS states are performed using the ORCA[54] package with different hybrid (B3LYP,[55–57] TPSSh[58]) and GGA functionals (PBE, BP86). The Ahlrichs basis sets have been employed: TZVP basis set[59] for all atoms and TZV/J auxiliary basis sets[60] as implemented in ORCA. The criteria for the SCF convergence are set as "TightSCF" (energy change $1e{-}08$; max-density change $1e{-}07$; rms-density change $5e{-}09$; DIIS error $5e{-}07$) and a high precision for the integration grids (Grid4) is used.

The geometry optimizations in EBS approach are produced interfacing the external optimizer features available in ORCA with an *ad hoc* C++ code. This code runs the HS and BS gradient calculations separately and uses Eqs. (8) and (10) to obtain the LS energy and forces as described in Subsection II B.

To evaluate the oxidation state of the transition metal atoms in all complexes we implemented the recent method proposed by Selloni and co-workers.[61] LS frequencies and normal modes are obtained from the LS energy Hessian matrix constructed around the optimized LS geometry combining the HS and LS Hessians as described in Eq. (11).

## III. RESULTS AND DISCUSSION

### A. Iron-sulfur clusters

The two-iron two-sulfur [2Fe–2S] cluster is an important inorganic component of several proteins involved in electron transfer processes. In Fd the [2Fe–2S] core is located inside its binding pocket anchored to four terminal-cysteines. We considered two models of this complex as shown in Figures 1(a) and 1(b).

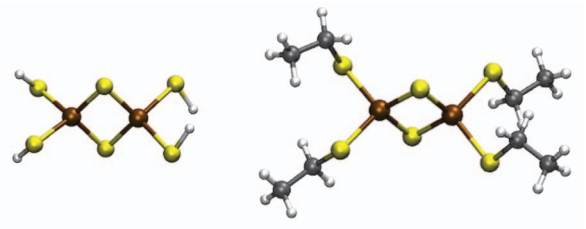

(a) (b)

FIG. 1. Molecular structures of ferredoxin core models employed in DFT calculations: (a) $[FE_2S_2(SH)_4]^{2-}$ and (b) $[FE_2S_2(SCH_2CH_3)_4]^{2-}$.

TABLE I. Structural properties and exchange coupling constant $J$ of models of [2Fe2S] core of ferredoxin using the extended broken symmetry approach in different computational schemes compared with protein experimental data.

| | Relaxed geometry | | | | AIMD (300 K) | | |
|---|---|---|---|---|---|---|---|
| **Low-spin state** | B3LYP[a,b] | PBE[a,b] | B3LYP[a,c] | PBE+U[b,d] | PBE+U[b,d] | PBE+U[d,e] | Exp.[e,f] |
| Fe–Fe (Å) | 2.81 | 2.65 | 2.79 | 2.7 | 2.75 | 2.74 | 2.75 |
| $S_1$–$S_2$ | 3.53 | 3.52 | 3.54 | ... | ... | ... | 3.52 |
| $Fe_1$–$S_1$ | 2.26 | 2.20 | 2.25 | 2.22 | 2.24 | 2.27 | 2.28 |
| $Fe_1$–$S_2$ | 2.26 | 2.20 | 2.25 | 2.22 | 2.24 | 2.22 | 2.23 |
| $Fe_2$–$S_1$ | 2.26 | 2.20 | 2.25 | 2.22 | 2.24 | 2.29 | 2.23 |
| $Fe_2$–$S_2$ | 2.26 | 2.20 | 2.25 | 2.23 | 2.24 | 2.24 | 2.18 |
| $S_1$–$Fe_1$–$S_2$ | 102.79 | 106.07 | 103.39 | ... | ... | ... | 102.2 |
| $S_1$–$Fe_2$–$S_2$ | 102.79 | 106.07 | 103.39 | ... | ... | ... | 105.6 |
| $Fe_1$–$S_1$–$Fe_2$ | 77.21 | 73.92 | 76.60 | 75.4 | 76.0 | 74.0 | 75.1 |
| $Fe_1$–$S_2$–$Fe_2$ | 77.21 | 73.92 | 76.62 | 75.3 | 76.0 | 76.0 | 76.8 |
| $S_2$–$Fe_1$–$S_1$—$Fe_2$ | 0.0 | 0.0 | −0.32 | 1.0 | 0.0 | 9.7 | 4.3 |
| $J$ ($cm^{-1}$) | −186 | –401 | −205 | −223 | −202(40) | −175 (35) | −182(20) |

[a]This work.
[b]From $[Fe_2S_2(SH)_4]^{2-}$ complex *in vacuo*.
[c]From $[Fe_2S_2(SCH_2CH_3)_4]^{2-}$ complex *in vacuo*.
[d]Several previous results: statics,[40] dynamics *in vacuo,*[38] and in oxidized *Anabaena* PCC7119 Fd protein.[40]
[e]From $[Fe_2S_2]Cys_4$ in protein.
[f]Structure data from x-ray diffraction in oxidized *Anabaena* PCC7119 Fd protein[62] and magnetic coupling constant from magnetic susceptibility calculation in *Spirulina maxima*[63] and Mössbauer spectroscopy from *spinach* protein.[64]

For each complex the geometry was optimized in the LS state according to the EBS forces using the B3LYP hybrid functional. The $J$ value was therefore evaluated at the LS minimum structures. Our results are summarized in Table I together with experimental data and previous theoretical calculations on similar complexes. In term of geometries and $J$ values we are in very close agreement to those obtained by Marx and co-workers using Hubbard correction on PBE functional. As discussed in their original paper,[40] they observe a dramatic improvement on the magnetic properties passing from PBE to PBE+U, thanks to the crucial role of the Hubbard repulsion term in avoiding the artificial spin density delocalization affecting local density approximation (LDA) and GGA calculations. Our structural results are in excellent agreement with the protein experimental data (Table I); the small differences can be attributed to the asymmetric deformation induced by the protein environment that breaks the planar ferredoxin core.

For the magnetic coupling constant $J$ we obtain a value which is in very good agreement with the experimental estimations and close to those obtained by DFT+U plane wave calculations. In comparing the results of our model with experiments we have to consider the influence of thermal fluctuations and the surrounding protein environment. This can be estimated by comparing statical (T = 0 K) dynamical (T = 300 K) and *in situ* molecular dynamics calculations performed in the same conditions with PBE+U[40] as reported in Table I. From this consideration we have to take into account a possible 20% variation which is anyway in line with DFT+U *ab-initio* molecular dynamics (AIMD) calculations and still in good agreement with experiments.

In conclusion, our results demonstrate how the EBS approach can be successfully used with B3LYP hybrid functional to obtain geometries and exchange coupling constants in good agreement with experimental data.

We also calculated the harmonic frequencies of the ferredoxin models in different spin states: HS, BS, and LS, as proposed in Subsection II C. The vibrational frequencies of the [2Fe–2S] core are reported in Table II together with the

TABLE II. Calculated vibrational harmonic frequencies ($cm^{-1}$) of Ferredoxin model *in vacuo*, compared with previous calculation from AIMD[39] and with experimental values of ferredoxin from *Porphyra umbilicalis*.[65]

| | (2Fe–2S)–4(SH) | | | | Real |
|---|---|---|---|---|---|
| Mode | BS B3LYP | HS B3LYP | LS B3LYP | LS PBE[a] | Exp. |
| $A_{g,A}$ | 144, 157, 290, 294 | 152, 288 | 288, 327 | 160 | 339[b] |
| $B_{1,g}$ | 269 | 233 | 372 | 318 | 329 |
| $B_{2u}$ | 325 | 260, 321 | 530 | 300–430, 396 | 426 |
| $A_{g,D}$ | 370 | 365 | 528 | 340, 364 | 395 |
| $B_{3u}$ | 382 | 355 | 293, 528 | 295 | 282[b], 367[b] |
| $B_{1u}$ | 290,144 | 132, 290 | 129, 279 | 145 | 357[c] |

[a]Frequencies from AIMD *in vacuo* by Ref. 39.
[b]Mode terminal dependent.
[c]Mode out of the plane of the 2Fe2S core (considered environment sensitive mode).

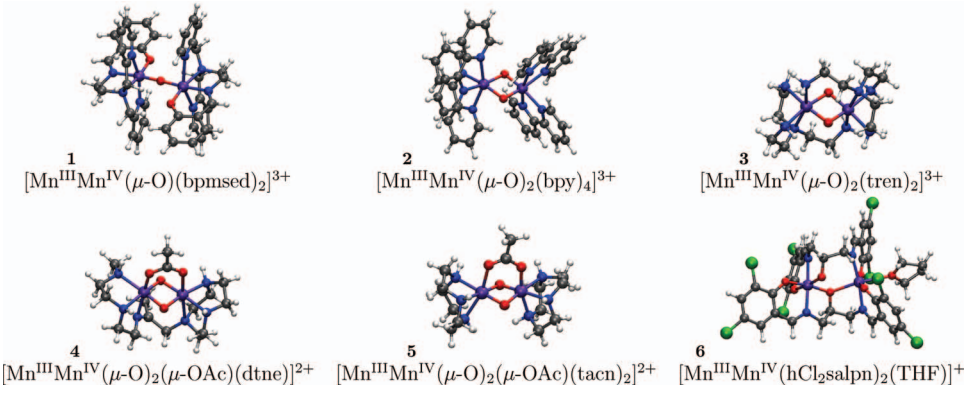


FIG. 2. Mixed-valence Mn(III)–Mn(IV) complexes optimized in their low-spin state by extended broken symmetry method.

experimental values and other theoretical frequencies calculated by *ab initio* molecular dynamics in gas phase.[39] The direct comparison with experiments in protein environment might be difficult for what concerns the $A_{g,A}$, $B_{3u}$, and $B_{1u}$ modes since they are either terminal modes or out-of-plane mode, therefore, supposed to be strongly influenced by the environment and by the tail termination. The other three modes report frequencies values in the range of the experiments, although all irregularly redshifted. With respect the HS and BS frequencies the LS results are in better agreement.

### B. Mixed-valence manganese dimers

The catalytic $Mn_4Ca$ complex of the oxygen evolving center (OEC) represents one of the major challenges for the electronic structure methods applied to biological systems. A recent crystal structure of OEC at atomic resolution[21] has opened the way to reliable quantum mechanics calculations to elucidate the mechanisms of the water splitting reaction. All the proposed reaction mechanisms[11,66] rely on reaction steps involving mixed-valence Mn intermediates. Discerning one proposal from another will be a difficult task for electronic structure calculations since an accurate description of mixed-valence cluster is required. The comparison between calculations and structural and electron paramagnetic resonance data available on di-nuclear Mn cluster offers a valuable opportunity to verify the accuracy and the consistency of different computational strategies. Neese and co-workers[42] for the case of a set of Mn(III)–Mn(IV) dimers successfully explored different DFT approaches using different functionals, BS strategies, and geometries.[42,67] In the present work we calculate the properties of several mixed-valence complexes evaluating the effect of the functional and the geometries on the exchange coupling constant. Moreover, we will use the EBS method to access the LS geometry and energy of the complexes. Six binuclear manganese complexes of mixed oxidation state (III/IV) are considered as shown in Figure 2.

We have optimized all geometries in several spin states, HS, BS, and LS, using different exchange-correlation functionals. The mixed-valence character of the complexes has been clearly recognized using the projection procedure described in Ref. 61. To evaluate the magnetic coupling constant we follow two different approaches: the first using the same functional and spin state as the one used in the geometry optimization, the second using different combination of functionals and geometries as reported in Ref. 42. The results using a geometry optimized in HS state, using BP86, a GGA functional, and afterwards calculating the exchange coupling

TABLE III. Exchange coupling constants $J$ (in $cm^{-1}$) for mixed-valence manganese(III/IV) complexes. Methods acronyms are in the form SS-F1/F2 where SS is the spin state (low spin, high spin, broken symmetry) and F1, F2 are the functionals used in geometry optimization and energy single point calculations, respectively.

| Method | 1 | 2 | 3 | 4 | 5 | 6 | $\langle\Delta J\rangle$ |
|---|---|---|---|---|---|---|---|
| Exp. | −177[a] | −150[b] | −146[c] | −110[d] | −110[e] | −10[f] | ... |
| LS-B3LYP/B3LYP | −169 | −142 | −125 | −104 | −111 | −8.9 | 7% |
| BS-B3LYP/B3LYP | −158 | −139 | −122 | −101 | −109 | −8.8 | 9% |
| HS-B3LYP/B3LYP | −115 | −127 | −112 | −82 | −102 | −8.0 | 21% |
| BS-BP86/B3LYP | −185 | −161 | −128 | −116 | −124 | −8.4 | 10% |
| HS-BP86/B3LYP | −101 | −123 | −106 | −80 | −99 | −7.0 | 26% |
| LS-TPSSh/TPSSh | −216 | −187 | −160 | −146 | −152 | −14.2 | 28% |
| BS-BP86/TPSSh | −218 | −210 | −160 | −145 | −157 | −11.3 | 27% |
| HS-BP86/TPSSh | −120 | −147 | −128 | −93 | −119 | −9.6 | 12% |

[a]Reference 68.
[b]Reference 69.
[c]Reference 70.
[d]Reference 71.
[e]Reference 72.
[f]References 73 and 74.

constant by other hybrid functional (B3LYP and TPSSh) are reported in Table III, labelled as HS-BP86/B3LYP and HS-BP86/TPSSh. As a second step we tried a similar mixed method, optimizing the geometry again with BP86 functional but in the antiferromagnetic BS electronic configuration (BS-BP86/B3LYP and BS-BP86/TPSSh in Table III). Broken-symmetry B3LYP geometric relaxations were also performed in both HS and BS states. Finally, we adopt the EBS method to optimize the geometry in the antiferromagnetic LS electronic configuration, using the hybrid functional B3LYP (or TPSSh) and obtaining the magnetic properties consistently with the same functional (LS-B3LYP/B3LYP and LS-TPSSh/TPSSh in Table III). The latter approach allows us to evaluate more easily the quality of the functional alone, since the geometries and the calculated $J$ are obtained in a consistent way. First we observe that the effects of the functional (BP86, B3LYP, or TPSSh) used to calculate the equilibrium geometry have a relevant influence on the metal-metal distances and angles, reflecting a dramatic variation on the calculated value of $J$.

The results for the exchange coupling constant are also compared with the experimental values and the quality of each approach is estimated using the relative $J$ error, defined as $\Delta \mathrm{J} = |(J_{\mathrm{th}} - J_{\mathrm{ex}})/J_{\mathrm{ex}}|$. This average quantity can be very useful to evaluate the accuracy of different methods in this kind of screening approach, as already shown.[42] The LS-B3LYP/B3LYP geometries gives a very good agreement with the available experimental data, reporting a $\Delta J$ as small as 7%. This result is close to what is obtained in the BS state (BS-B3LYP/B3LYP), at variance with the HS-B3LYP/B3LYP which is rather off the experimental values (21%). Beyond the better agreement with experiments of our proposed LS-B3LYP/B3LYP scheme, we wish to remark the fact that in our approach geometries and magnetic properties (which rely on calculations of energy differences) are calculated consistently using the same functionals on the low-spin ground state of the effective spin Hamiltonian (Eq. (1)). A comparison between the results obtained with the two hybrid functionals (B3LYP and TPSSh), considering the same geometry (HS-BP86 or BS-BP86), suggests an over estimation of $J$ for TPSSh over B3LYP. Table III also shows the influence of the spin state on the evaluation of $J$, reporting smaller values for equilibrium geometries in the HS state with respect to those in LS and BS states. This is in agreement with the observation that HS metal-metal distances are usually larger, therefore leading to a smaller magnetic coupling. The above effects may compensate each other in some extent when TPSSh calculations are performed on HS geometries (for instance, using BP86 functional), eventually leading to a good estimate of $J$, as shown in the last line of Table III and reported already by Neese and co-workers[42] for a similar class of complexes.

## IV. CONCLUSIONS

In the present work we have applied for the first time the EBS method in combination with hybrid functionals to di-nuclear transition metal complexes. An extensive comparison of distances and magnetic coupling constants on ferredoxin molecular models indicates that EBS-B3LYP leads to results in very good agreements with experimental data, similar to what obtained using the DFT+U approach on the same systems.[40] We have used the EBS formalism for Hessian calculation and normal mode analysis around the low-spin relaxed geometries of the ferrodoxin models, comparing the obtained frequencies with the experimental data available for the full protein. The performance of the proposed approach to mixed-valence Mn(III)–Mn(IV) dimers, was inferred by comparing the EBS method using two hybrid functionals (B3LYP and TPSSh) with the results obtained on broken-symmetry and high-spin geometries. Calculations performed on 6 different mixed-valence clusters demonstrate that EBS-B3LYP provides an accurate estimation of the exchange coupling constant $J$, being the average discrepancy with experimental values as small as 7%. Beyond the fair comparison with the experiments, our scheme represents a consistent way to evaluate $J$ since the energy differences are evaluated on the low-spin geometry with the same functional used for the optimization. This work represents the first step towards an accurate study by DFT of the low-spin state of larger multi-centers mixed-valence Mn compounds such as the catalytic cluster of the oxygen evolving complex in Photosystem II.

## ACKNOWLEDGMENTS

We acknowledge CASPUR and CINECA supercomputing centers for computational resources. We are grateful to Dimitrios Pantazis for useful discussions, to Donato Pera and Piergiacomo De Ascaniis for their technical support at the Caliban-HPC Laboratory of the University of L'Aquila, and to Daniele Varsano and Matteo Barborini for a critical reading of the paper. We acknowledge funding provided by the European Research Council Project No. 240624 "MultiscaleChemBio" within the VII Framework Program of the European Union (EU).

[1] H. Beinert, R. H. Holm, and E. Munck, Science **277**, 653–659 (1997).
[2] D. C. Rees and J. B. Howard, Science **300**, 929–931 (2003).
[3] D. C. Johnson, D. R. Dean, A. D. Smith, and M. K. Johnson, Annu. Rev. Biochem. **74**, 247–281 (2005).
[4] R. Cammack, D. S. Patil, E. C. Hatchikian, and V. M. Fernandez, Biochim. Biophys. Acta **912**, 98–109 (1987).
[5] M. W. W. Adams, Biochim. Biophys. Acta **1020**, 115–145 (1990).
[6] M. Wang, L. Chen, X. Li, and L. Sun, Dalton Trans. **40**, 12793–12800 (2011).
[7] S. Foerster, M. Stein, M. Brecht, H. Ogata, Y. Higuchi, and W. Lubitz, J. Am. Chem. Soc. **125**, 83–93 (2003).
[8] A. C. Rosenzweig and M. H. Sazinsky, Curr. Opin. Struct. Biol. **16**, 729–735 (2006).
[9] K. N. Ferreira, T. M. Iverson, K. Maghlaoui, J. Barber, and S. Iwata, Science **303**, 1831–1838 (2004).
[10] M. Kusunoki, Biochim. Biophys. Acta Bioenerg. **1767**, 484–492 (2007).
[11] P. Gatt, R. Stranger, and R. J. Pace, J. Photochem. Photobiol., B **104**, 80–93 (2011).
[12] A. Baron, C. Herrero, A. Quaranta, M.-F. Charlot, W. Leibl, B. Vauzeilles, and A. Aukauloo, Chem. Commun. **47**, 11011–11013 (2011).
[13] B. Chiavarino, M. E. Crestoni, and S. Fornarini, Chemistry **8**, 2740–2746 (2002).
[14] A. Magnuson, M. Anderlund, O. Johansson, P. Lindblad, R. Lomoth, T. Polivka, S. Ott, K. Stensjo, S. Styring, V. Sundström, and L. Hammarstrom, Acc. Chem. Res. **42**, 1899–1909 (2009).
[15] S. I. Allakhverdiev, V. D. Kreslavski, V. Thavasi, S. K. Zharmukhamedov, V. V. Klimov, T. Nagata, H. Nishihara, and S. Ramakrishna, Photochem. Photobiol. Sci. **8**, 148–156 (2009).
[16] F. Neese, J. Biol. Inorg. Chem. **11**, 702–711 (2006).
[17] F. Neese, Coord. Chem. Rev. **253**, 526–563 (2009).

[18]I. Rudra, Q. Wu, and T. van Voorhis, J. Chem. Phys. **124**, 024103 (2006).
[19]S. Luo, I. Rivalta, V. S. Batista, and D. G. Truhlar, J. Phys. Chem. Lett. **2**, 2629–2633 (2011).
[20]W. Ames, D. A. Pantazis, V. Krewald, N. Cox, J. Messinger, W. Lubitz, and F. Neese, J. Am. Chem. Soc. **133**, 19743–19757 (2011).
[21]Y. Umena, K. Kawakami, J.-R. Shen, and N. Kamiya, Nature (London) **473**, 55–U65 (2011).
[22]G. Mattioli, M. Risch, A. A. Bonapasta, H. Dau, and L. Guidoni, Phys. Chem. Chem. Phys. **13**, 15437–15441 (2011).
[23]R. Neumann, R. H. Nobes, and N. C. Handy, Mol. Phys. **87**, 1–36 (1996).
[24]A. Cohen, P. Mori-Sanchez, and W. Yang, Science **321**, 792 (2008).
[25]A. Bencini, Inorg. Chim. Acta **361**, 3820–3831 (2008).
[26]F. Neese, T. Petrenko, D. Ganyushin, and G. Olbrich, Coord. Chem. Rev. **251**, 288–327 (2007).
[27]R. Valero, R. Costa, I. P. R. Moreira, D. G. Truhlar, and F. Illas, J. Chem. Phys. **128**, 114103 (2008).
[28]C. J. Barden, J. C. Rienstra-Kiracofe, and H. F. Schaefer, J. Chem. Phys. **113**, 690–700 (2000).
[29]Y. Zhao and D. G. Truhlar, Theor. Chem. Acc. **120**, 215–241 (July 2008).
[30]V. I. Anisimov, F. Aryasetiawan, and A. I. Lichtenstein, J. Phys.: Condens. Matter **9**, 767–808 (1997).
[31]M. Cococcioni and S. de Gironcoli, Phys. Rev. B **71**, 035105 (2005).
[32]H. J. Kulik, M. Cococcioni, D. A. Scherlis, and N. Marzari, Phys. Rev. Lett. **97**, 103001 (2006).
[33]C. Cao, S. Hill, and H.-P. Cheng, Phys. Rev. Lett. **100**, 167206 (2008).
[34]S. A. Fiethen, V. Staemmler, N. N. Nair, J. Ribas-Arino, E. Schreiner, and D. Marx, J. Phys. Chem. B **114**, 11612–11619 (2010).
[35]L. Noodleman, J. Chem. Phys. **74**, 5737–5743 (1981).
[36]L. Noodleman and E. R. Davidson, Chem. Phys. **109**, 131–143 (1986).
[37]X. G. Zhao, W. H. Richardson, J. L. Chen, J. Li, L. Noodleman, H. L. Tsai, and D. N. Hendrickson, Inorg. Chem. **36**, 1198–1217 (1997).
[38]E. Schreiner, N. N. Nair, R. Pollet, V. Staemmler, and D. Marx, PNAS **104**, 20725 (2007).
[39]N. N. Nair, E. Schreiner, R. Pollet, V. Staemmler, and D. Marx, J. Chem. Theory Comput. **4**, 1174–1188 (2008).
[40]N. N. Nair, J. Ribas-Arino, V. Staemmler, and D. Marx, J. Chem. Theory Comput. **6**, 569–575 (2010).
[41]Md. E. Ali, N. N. Nair, V. Staemmler, and D. Marx, J. Chem. Phys. **136**, 224101 (2012).
[42]M. Orio, D. A. Pantazis, T. Petrenko, and F. Neese, Inorg. Chem. **48**, 7251–7260 (2009).
[43]W. Heisenberg, Z. Phys. **49**, 619–636 (1928).
[44]P. Dirac, Proc. R. Soc. London, Ser. A **123**, 714–733 (1929).
[45]J. H. van Vleck, Science **76**, 326 (1932).
[46]When the Heisenberg exchange is not dominant we need to account for the zero-field splitting (ZFS) contribution adding a new term in Eq. (1), $H = -2J\hat{S}_A \cdot \hat{S}_B + \hat{S}_A \cdot \tilde{D}^{(A)} \cdot \hat{S}_A + \hat{S}_B \cdot \tilde{D}^{(B)} \cdot \hat{S}_B$, where $\tilde{D}^{(i)}$ is the local ZFS tensor for site $i$. For the mixed-valence Mn dimer the $J$ value of the strong exchange limit was established[42] to be approximately $J < -75\ \mathrm{cm}^{-1}$.
[47]S. Sinnecker, F. Neese, L. Noodleman, and W. Lubitz, J. Am. Chem. Soc. **126**, 2613–2622 (2004).
[48]S. Sinnecker, F. Neese, and W. Lubitz, J. Biol. Inorg. Chem. **10**, 231–238 (2005).
[49]P. Löwdin, Phys. Rev. **97**, 1474–1489 (1955).
[50]F. Neese, J. Phys. Chem. Solids **65**, 781–785 (2004).
[51]K. Yamaguchi, H. Fukui, and T. Fueno, Chem. Lett. **1986**, 625–628 (1986).
[52]M. Nishino, S. Yamanaka, Y. Yoshioka, and K. Yamaguchi, J. Phys. Chem. A **101**, 705–712 (1997).
[53]Here it is assumed that $n^{\alpha}_{\mathrm{mag}} \geq n^{\beta}_{\mathrm{mag}}$ without loss of generality.
[54]F. Neese, ORCA, version 2.6-35, an *ab initio* density functional and semiempirical program package, Universität Bonn, Bonn, Germany, 2007; F. Neese, "Spin Hamiltonian Parameters from First Principle Calculations: Theory and Application," in *Biological Magnetic Resonance*, Vol. 28, edited by G. Hanson and L. Berliner (Springer, 2008), pp. 175–232.
[55]A. D. Becke, Phys. Rev. A **38**, 3098–3100 (1988).
[56]C. Lee, W. Yang, and R. G. Parr, Phys. Rev. B **37**, 785–789 (1988).
[57]A. D. Becke, J. Chem. Phys. **98**, 5648–5652 (1993).
[58]V. N. Staroverov, G. E. Scuseria, J. M. Tao, and J. P. Perdew, J. Chem. Phys. **119**, 12129–12137 (2003).
[59]A. Schäfer, H. Horn, and R. Ahlrichs, J. Chem. Phys. **97**, 2571–2577 (1992).
[60]F. Weigend, Phys. Chem. Chem. Phys. **8**, 1057–1065 (2006).
[61]P. H. L. Sit, R. Car, M. H. Cohen, and A. Selloni, Inorg. Chem. **50**, 10259–10267 (2011).
[62]R. Morales, M. H. Chron, G. Hudry-Clergeon, Y. Petillot, S. Norager, M. Medina, and M. Frey, Biochemistry **38**, 15764–15773 (1999).
[63]L. Petersson, Biochim. Biophys. Acta (BBA) - Protein Struct. **622**, 18–24 (1980).
[64]G. Palmer, W. R. Dunham, J. A. Fee, R. H. Sands, T. Lizuka, and T. Yonetani, Biochim. Biophys. Acta (BBA) - Bioenergetics **245**, 201–207 (1971).
[65]F. A. Rotsaert, J. D. Pikus, B. G. Fox, J. L. Markley, and J. Sanders-Loehr, J. Biol. Inorg. Chem. **8**, 318–326 (2003).
[66]P. E. M. Siegbahn, Acc. Chem. Res. **42**, 1871–1880 (2009).
[67]S. Yamanaka, K. Kanda, T. Saito, Y. Kitagawa, T. Kawakami, M. Ehara, M. Okumura, H. Nakamura, and K. Yamaguchi, Chem. Phys. Lett. **519–520**, 134–140 (2012).
[68]O. Horner, E. Anxolabehere-Mallart, M. F. Charlot, L. Tchertanov, J. Guilhem, T. A. Mattioli, A. Boussac, and J. J. Girerd, Inorg. Chem. **38**, 1222–1232 (1999).
[69]A. F. Jensen, Z. W. Su, N. K. Hansen, and F. K. Larsen, Inorg. Chem. **34**, 4244–4252 (1995).
[70]K. S. Hagen, W. H. Armstrong, and H. Hope, Inorg. Chem. **27**, 967–969 (1988).
[71]K. O. Schäfer, R. Bittl, W. Zweygart, F. Lendzian, G. Haselhorst, T. Weyhermüller, K. Wieghardt, and W. Lubitz, J. Am. Chem. Soc. **120**, 13104–13120 (1998).
[72]K. Wieghardt, U. Bossek, L. Zsolnai, G. Huttner, G. Blondin, J. J. Girerd, and F. Babonneau, J. Chem. Soc., Chem. Commun. **1987**, 651–653 (1987).
[73]E. Larson, A. Haddy, M. L. Kirk, R. H. Sands, W. E. Hatfield, and V. L. Pecoraro, J. Am. Chem. Soc. **114**, 6263–6265 (1992).
[74]M. Zheng, S. V. Khangulov, G. C. Dismukes, and V. V. Barynin, Inorg. Chem. **33**, 382–387 (1994).